Clinical and Translational Science

ARTICLE OPEN ACCESS

Radiolabelled Cyclodextrins for the Positron Emission Tomography Imaging of Breast Cancer: Preclinical Perspectives

Tamás Sass[1,2] | Judit P. Szabó[3] | Renáta Adél Dienes[2,3] | Péter Árkosy[4] | Gábor Opposits[3] | István Jószai[3] | Anikó Fekete[3] | Ferenc Fenyvesi[5] | István Hajdu[3] | György Trencsényi[2,3] | Zita Képes[2,3]

[1]Department of Surgery, Faculty of Medicine, University of Debrecen, Debrecen, Hungary | [2]Gyula Petrányi Doctoral School of Clinical Immunology and Allergology, Faculty of Medicine, University of Debrecen, Debrecen, Hungary | [3]Division of Nuclear Medicine and Translational Imaging, Department of Medical Imaging, Faculty of Medicine, University of Debrecen, Debrecen, Hungary | [4]Department of Oncology, Faculty of Medicine, University of Debrecen, Debrecen, Hungary | [5]Department of Molecular and Nanopharmaceutics, Faculty of Pharmacy, University of Debrecen, Debrecen, Hungary

Correspondence: Zita Képes (kepes.zita@med.unideb.hu)

Received: 29 April 2025 | **Revised:** 27 August 2025 | **Accepted:** 26 September 2025

Funding: This study was supported by the OTKA K-147308 research grant of the National Research, Development and Innovation Office, Budapest, Hungary.

Keywords: angiogenesis | breast cancer | cyclodextrin | positron emission tomography | preclinical | prostaglandin E2 | radiopharmaceuticals

ABSTRACT

Given the increasing incidence and mortality of breast cancer, the development of target-specific imaging probes for early disease detection seems straightforward. Prostaglandin E2 (PGE2) and its receptors have a crucial role in tumor angiogenesis; therefore, radiolabelled cyclodextrins targeting such biomolecules may serve as selective vectors for positron emission tomography (PET) imaging of breast cancer. Herein, we aimed to monitor PGE2 production in MDA-MB-HER2-positive and 4T1 triple-negative breast cancer xenografts using ^{68}Ga-labeled randomly methylated beta cyclodextrin (RAMEB) and 2-hydroxypropyl-beta-cyclod extrin (HPβCD) and PET technique. After the injection of [^{68}Ga]Ga-NODAGA-HPβCD and [^{68}Ga]Ga-DOTAGA-RAMEB, CB17 SCID mice bearing breast tumors underwent weekly PET imaging with subsequent quantitative data assessment and ex vivo biodistribution studies. Both cyclodextrin compounds were suitable to identify the tumors, though tracer accumulation varied with tumor size. Significantly higher [^{68}Ga]Ga-NODAGA-HPβCD uptake was observed in the MDA-MB-HER2+ tumors across all sizes (small, medium, and large-sized) compared to the 4T1 counterparts. In contrast, [^{68}Ga]Ga-DOTAGA-RAMEB accumulated to a greater extent in small and midsized 4T1 tumors in comparison with size-matched MDA-MB-HER2+ tumors, while it showed higher uptake in the large HER2+ lesions than in 4T1. The presented results indicate notable radioactivity in both 4T1 and MDA-MB-HER2+ tumors designating [^{68}Ga]Ga-DOTAGA-RAMEB and [^{68}Ga]Ga-NODAGA-HPβCD as effective PET probes for the identification of breast cancer.

1 | Introduction

Despite recent therapeutic advancements, breast cancer remains one of the most common malignancies among women worldwide [1, 2]. Given its increasing global incidence and mortality [3], early diagnosis is imperative to improve patient outcomes and survival [4, 5].

The non-invasive nature of nuclear medical positron emission tomography/computed tomography (PET/CT) (using

György Trencsényi and Zita Képes contributed equally to the present work.

Study Highlights

- What is the current knowledge on the topic?
  - Despite recent therapeutic advancements, breast cancer still remains one of the most common malignancies among women. Therefore, the development of target-specific diagnostic probes that allow for early detection and therapeutic intervention seems straightforward.
- What question did this study address?
  - In this study, we tested and compared the in vivo diagnostic capability of two ^{68}Ga-labeled cyclodextrin radiopharmaceuticals—[^{68}Ga]Ga-NODAGA-HPβCD and [^{68}Ga]Ga-DOTAGA-RAMEB—in breast cancer imaging using MDA-MB-HER2+ and triple-negative 4T1 breast cancer xenografts and positron emission computed tomography (PET) technique.
- What does this study add to our knowledge?
  - This was the first study to prove the diagnostic ability of radiolabelled cyclodextrin compounds in the in vivo PET detection of breast tumors.
- How might this change clinical pharmacology or translational science?
  - These carbohydrate-based radiotracers have the potential to evolve as valuable complementary diagnostic probes to the already established breast-specific tracers. Therefore, their integration into routine oncological imaging may contribute to the establishment of personalized diagnostics and medicine.

radiopharmaceuticals) offers a reassuring approach for early detection of breast cancer signs [6–8]. Even though fluorine-18-2-fluoro-2-deoxy-D-glucose ([^{18}F]FDG) PET/CT continues to be the gold standard for staging, restaging, and treatment follow-up [9, 10], novel breast-specific imaging probes [11, 12] have emerged to bypass the limitations of [^{18}F]FDG [13–15]. Tumor-selective radiopharmaceuticals targeting cell surface receptors—such as human epidermal growth factor receptor (^{89}Zr-cetuximab [16]), estrogen receptor alpha (^{18}F-fluoroestradiol/[^{18}F]F-FES, [17]), and tissue factor (TF) (^{64}Cu-labeled anti-TF antibody/^{64}Cu-NOTA-ALT-836 [18]), or upregulated glycoproteins including Mucin 1 (MUC1) (^{99}Tc-labeled MUC1 peptide [19]) and CD146 transmembrane glycoprotein ([^{52}Mn]Mn-DOTA-YY146 [20]) have been established as strong applicants for use in breast cancer molecular imaging. Beyond these tumor-specific compounds, significant advancements have been made in developing radiotracers targeting the tumor microenvironment [11]. Recent studies reported promising results for fibroblast activation protein (FAPI)-specific PET probes ([^{68}Ga]Ga-FAPI-46 [21]) targeting FAPI positive peritumoral fibroblasts [22] or hypoxia-specific radiomarkers (^{18}F-labeled fluoromisonidazole/[^{18}F]F-FMISO [23]). Nevertheless, hypoxia-PET is a highly desirable indirect method for angiogenesis imaging [24, 25], direct agents such as radiolabeled ligands of a_vb_3 integrin [26] or the vascular endothelial growth factor/receptor (VEGF-A/B, VEGFR) ([^{89}Zr]Zr-DFO-bevacizumab [27]) seem more specific [28] in angiogenesis imaging associated with breast carcinogenesis. Given the high expression of prostaglandin E2 (PGE2) and PGE2 receptors in breast malignancies [29], these pro-angiogenic molecules serve as novel targets for direct angiogenesis imaging. Cyclodextrin oligosaccharides showing selective affinity to PGE2 [30, 31], although still in their early stage of development, have already proved their preclinical capability to detect PGE2$^+$ malignancies [32, 33]. Randomly methylated beta cyclodextrin (RAMEB) or 2-Hydroxypropyl-beta-cyclodextrin (HPβCD) radiolabeled with ^{68}Ga, ^{213}Bi or ^{52}Mn isotopes could be successfully used for the visualization of PGE2$^+$ tumor models including, among others, HT1080 human fibrosarcoma, BxPC3 human pancreatic adenocarcinoma, B16F10 mouse melanoma, or mesoblastic nephroma (Ne/De) [33–36].

Overall, we suggested that vascular-homing with radiolabelled cyclodextrin derivatives could be a useful companion tool in detecting angiogenic processes in breast cancer. Hence, in this study we tested and compared the in vivo diagnostic ability of ^{68}Ga-labeled RAMEB and HPβCD radiopharmaceuticals ([^{68}Ga]Ga-NODAGA-HPβCD and [^{68}Ga]Ga-DOTAGA-RAMEB) applying MDA-MB-HER2+ and triple-negative 4T1 breast cancer xenografts and PET technique.

2 | Materials and Methods

2.1 | Cell Culturing

MDA-MB-HER2+ and 4T1 triple negative breast cancer cells from ATCC (American Type Culture Collection, Manassas, VA, USA) were cultivated as recommended by the distributor.

To ensure adherent, monolayer growth, MDA-MB-HER2+ cells were grown in a monolayer culture in Dulbecco's Modified Eagle Medium (DMEM) supplemented with 10% heat-inactivated fetal bovine serum (FBS) and 1% antibiotic solution (Sigma-Aldrich Ltd., St. Louis, Missouri, United States) at 37°C in a 5% CO_2 humidified atmosphere (ESCO CCl-170B-8 incubator, Esco Micro Pte. Ltd., Singapore). Cells were passed 3 times a week after reaching 80% confluence.

The 4T1 cell line was maintained in RPMI-1640 media + 10% heat-inactivated FBS (12 mL per T-75 flasks) and incubated under the same conditions as MDA-MB-HER2+ cells. Subculturing was performed every 2–3 days at 80% confluence.

Tumor cells were used for further experiments after 5-to-8 passages. Prior to transplantations, a Bürker chamber was used for counting, and viability was assessed with the trypan blue dye exclusion test. Thereafter, we set the desired cell concentration for tumor generation.

2.2 | Animal Studies

All animal procedures were approved by the Ethics Committee of the University of Debrecen (permission number: 16/2020/DEMÁB) and conducted in compliance with all applicable sections of Hungarian law and the directions and regulations of the European Union.

2.2.1 | Breast Carcinoma Model Establishment

Thirty-six CB17 severe combined immunodeficient (SCID) female mice (12 weeks old, weighing approx. 20 g) purchased from Innovo Ltd. (Isaszeg, Hungary) were used for tumor model establishment. All experimental animals were treated according to the European acts (Directive 2010/63/EU) and housed under a sterile laboratory environment in individually ventilated cages (IVC, Tecniplast, Buguggiate, Italy) at 26°C ± 3°C with 55% ± 10% relative humidity. Artificial lighting with 12-h light/dark cycles and sterile semi-synthetic food (Akronom Ltd., Budapest, Hungary) with tap water were provided *ad libitum*.

To create tumor-bearing models, a total of 5×10^6 MDA-MB-HER2+ or 4T1 cells in 100–120 μL of DMEM:Matrigel mixture (1:1) were subcutaneously injected into the left shoulder area of each mouse ($n = 18$ 4T1, $n = 18$ MDA-MB-HER2+). During tumor induction, isoflurane-induced anesthesia (3% Aerrane, Baxter Hungary Ltd., Budapest, Hungary, (OGYI-T-08993), 0.4 L/min O_2, 1.2 L/min N_2O) was used and maintained with a dedicated small animal inhalation anesthesia device (Tec3 Isoflurane Vaporizer, Eickemeyer Veterinary Equipment, Luton, UK). Post tumor generation, caliper measurements were applied to follow tumor growth weekly. Tumor volumes were calculated using the equation $V = (L*W^2)/2$ where V, L, and W stand for tumor volume (mm^3), tumor length (mm), and tumor width (mm), respectively.

2.2.2 | Preclinical PET Imaging and Ex Vivo Organ Distribution Studies

[^{68}Ga]Ga-NODAGA-HPβCD and [^{68}Ga]Ga-DOTAGA-RAMEB were synthesized in accordance with a previously described method [32, 33].

After the tumors became visible, [^{68}Ga]Ga-NODAGA-HPβCD and [^{68}Ga]Ga-DOTAGA-RAMEB micro-PET imaging was performed weekly with all tumor-bearing mice, with the two tracers administered on consecutive days ($n = 9$ 4T1, $n = 9$ MDA-MB-HER2+). Sixty min post injection of approximately 8–10 MBq of [^{68}Ga]Ga-NODAGA-HPβCD in 100–150 μL physiological saline, static PET acquisition (20 min) was conducted using the MiniPET-II scanner of the Preclinical Laboratory of the Division of Nuclear Medicine and Translational Imaging, Department of Medical Imaging, Faculty of Medicine, University of Debrecen (Debrecen, Hungary), which was followed by [^{68}Ga]Ga-DOTAGA-RAMEB PET imaging a day later based on the same protocol.

All procedures were done under isoflurane-induced anesthesia (3% Aerrane, 0.4 L/min O_2, 1.2 L/min N_2O) using the same animal inhalation device.

As part of quantitative PET data assessment, volumes of interest (VOI) were manually outlined on the PET scan of each tumor; then, using the following formula, the mean standardized uptake values (SUVmean expressed in g/mL) were determined with BrainCad image analyses software (University of Debrecen, Debrecen, Hungary):

$$\mathrm{SUV} = \frac{\text{activity concentration within the VOI (MBq / mL)}}{\text{injected dose (MBq) / body weight (g)}}$$

To analyze cyclodextrin uptake changes related to tumor development ex vivo biodistribution studies were performed at the same time points as PET imaging ($n = 9$/group). Mice were sacrificed 60 min after the administration of 8–10 MBq of [^{68}Ga]Ga-NODAGA-HPβCD or [^{68}Ga]Ga-DOTAGA-RAMEB (in 100–150 μL physiological saline). All tumors were removed, weighed wet and measured for radioactivity using gamma counting (Perkin-Elmer Packard Cobra, Waltham, MA, USA). The radioactive uptake rate of the tumor tissue was calculated after radioactivity decay correction and expressed as %ID/g.

2.3 | Statistical Analysis

Statistical analysis was performed using MedCalc 18.5 (MedCalc Software, Mariakerke, Belgium). Two-sample *t*-test, two-way analysis of variance/ANOVA, and the Mann–Whitney *U* test were used for group comparison based on data normality and homogeneity. We considered $p < 0.05$ as statistically significant. Descriptive statistics are presented as mean ± SD.

3 | Results

3.1 | In Vivo PET Results

The diagnostic capability of [^{68}Ga]Ga-DOTAGA-RAMEB and [^{68}Ga]Ga-NODAGA-HPβCD was assessed and compared in mice bearing subcutaneous MDA-MB-HER2+ and 4T1 tumors using the PET technique. Tumor induction was 100% successful, as all inoculated animals developed palpable tumors. Consequently, all mice were included in the in vivo PET imaging studies.

3.1.1 | MDA-MB-HER2+ Tumors

As presented by Figure 1, both tracers primarily accumulated in the tumors and the kidneys, indicating renal clearance. Beyond the meaningful renal uptake, the PET images demonstrated detectable tumor uptake at all experimental time points for both radiopharmaceuticals (Figure 1, Panels A and B) with a gradual increase over time—especially in the case of the RAMEB molecule between Days 50 and 65 (Figure 1, Panel B). Even though the tumors could be clearly visualized at all three time points, on the [^{68}Ga]Ga-DOTAGA-RAMEB PET scans, considerable background noise was observed. In contrast, for the HPβCD derivative, hardly any activity was registered in the investigated abdominal and thoracic organs, enabling clear lesion delineation (Figure 1, Panel A).

In line with the qualitative assessment, quantitative PET analysis also confirmed that both cyclodextrin derivatives exhibited effective binding to the HER2+ neoplasms (Figure 2 and Table S1). In addition, SUV data (expressed in g/mL) showed steadily rising tracer concentrations for both radiopharmaceuticals until the end of the experiment (Figure 2) with respective values being 0.04 ± 0.006, 0.06 ± 0.015, and 0.07 ± 0.013 for [^{68}Ga]Ga-NODAGA-HPβCD, and 0.02 ± 0.003, 0.03 ± 0.005, and 0.06 ± 0.009 for the RAMEB derivative 35, 50, and 65 days post tumor establishment. These results correlated with the visual observations. Comparing the MDA-MB-HER2+ tumor

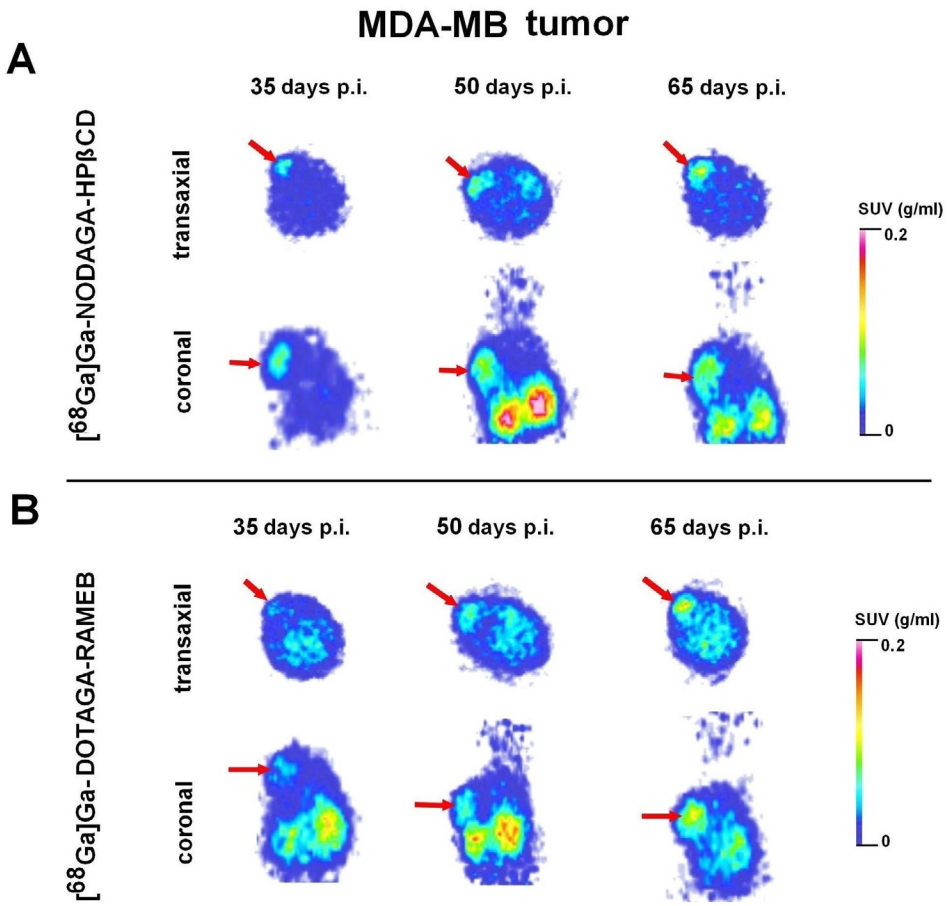

FIGURE 1 | In vivo PET imaging of MDA-MB-HER2+ tumor-bearing mice. Representative, decay-corrected PET images of the MDA-MB-HER2+ tumor-bearing mice 35, 50, 65 days after tumor cell transplantation and 60 min post injection of [^{68}Ga]Ga-NODAGA-HPβCD (Panel A) and [^{68}Ga]Ga-DOTAGA-RAMEB (Panel B). Red arrows: Subcutaneously growing tumors. p.i., Post MDA-MB-HER2+ tumor cell inoculation.

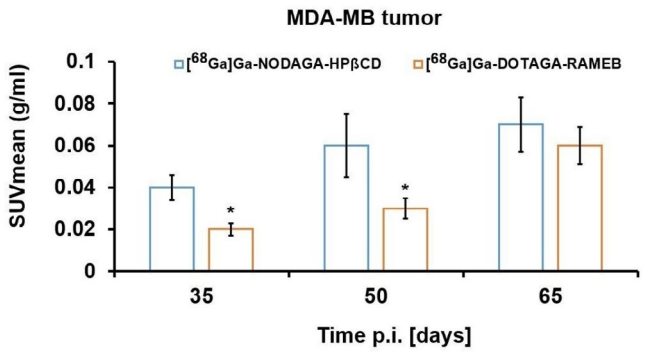

FIGURE 2 | Quantitative PET analysis of mice bearing MDA-MB-HER+ tumors. Quantitative SUV analysis in CB17 SCID mice bearing MDA-MB-HER2+ tumors 35, 50, and 65 days post tumor cell transplantation and 60 min after the tail vein injection of [^{68}Ga]Ga-NODAGA-HPβCD and [^{68}Ga]Ga-DOTAGA-RAMEB. All values are displayed as mean ± SD. $p \leq 0.05$ (*). $n = 3$ tumor-bearing mice/radiopharmaceutical/time point. The respective SUV values (expressed in g/ml) were 0.04 ± 0.006, 0.06 ± 0.015, and 0.07 ± 0.013 for the [^{68}Ga]Ga-NODAGA-HPβCD radiotracer 35, 50, and 65 days post tumor establishment, and 0.02 ± 0.003, 0.03 ± 0.005, and 0.06 ± 0.009 for the RAMEB derivative at the same time points. p.i., post injection of MDA-MB-HER2+ tumor cells; SUV, standardized uptake value.

concentrations of the two cyclodextrin radioprobes, at Days 35 and 50, the uptake of the HPβCD compound was significantly higher compared to the RAMEB molecule, but by Day 65, this difference was no longer statistically significant *($p \leq 0.05$)*.

3.1.2 | 4T1 Tumors

Visually, all tumors could be clearly delineated with both cyclodextrin probes at all three experimental days; however, the tumor uptake was generally more elevated using the ^{68}Ga-labeled RAMEB molecule, especially at the 20th day (Figure 3). In addition, continuously increasing tracer accumulations were detected for both radiopharmaceuticals over the experimental period, with the RAMEB compound showing more pronounced uptake.

Similarly to the visual experiences, both [^{68}Ga]Ga-NODAGA-HPβCD and [^{68}Ga]Ga-DOTAGA-RAMEB PET evidenced strong and specific uptake in the 4T1 tumors with increasing signal intensity over time. The corresponding SUV values (expressed in g/mL) for [^{68}Ga]Ga-NODAGA-HPβCD were 0.02 ± 0.003, 0.03 ± 0.006, and 0.035 ± 0.004 at 10, 15, and 20 days after tumor cell transplantation, and for [^{68}Ga]Ga-DOTAGA-RAMEB, the

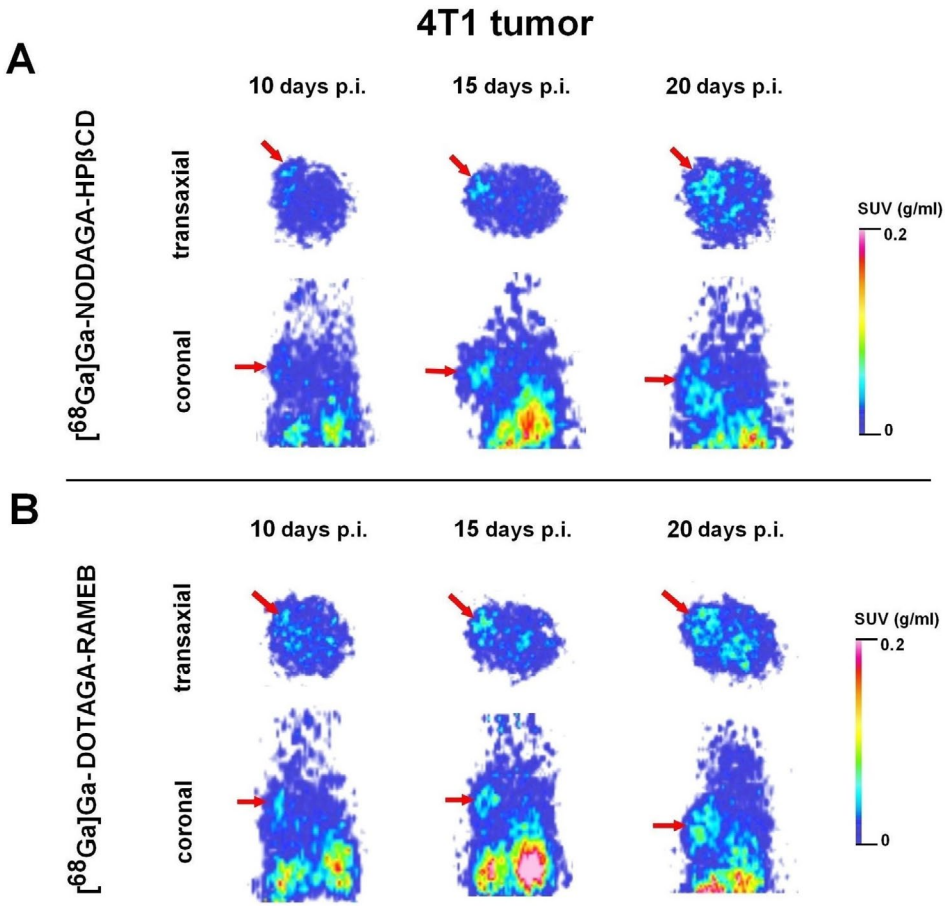

FIGURE 3 | In vivo PET imaging of triple negative 4T1 tumor-bearing mice. Representative, decay-corrected [^{68}Ga]Ga-NODAGA-HPβCD (Panel A) and [^{68}Ga]Ga-DOTAGA-RAMEB (Panel B) PET images in 4T1 tumors 10, 15 and 20 days post tumor cell injection and 60 min after tracer administration. Red arrows indicate the subcutaneously growing tumors. p.i., post injection of 4T1 tumor cells.

values were 0.025 ± 0.002, 0.034 ± 0.004, and 0.04 ± 0.005 at the same time points (see Figure 4 and Table S2). Head-to-head comparison revealed slightly higher accumulation for the RAMEB compound at all experimental days; however, this difference was statistically not considerable at any of the time points.

3.2 | Ex Vivo Studies

Ex vivo organ distribution studies were performed to support the micro-PET imaging results. Biodistribution data of [^{68}Ga]Ga-NODAGA-HPβCD and [^{68}Ga]Ga-DOTAGA-RAMEB in 4T1 tumor-bearing mice are summarized in Table S3 and Figure 5 Panel A. The 4T1 tumors showed gradually increasing uptake of both tracers between days 10 and 15 post tumor induction (Figure 5, Table S3). A peak uptake on Day 15 ([^{68}Ga]Ga-DOTAGA-RAMEB: 3.10% ± 0.45%ID/g, [^{68}Ga]Ga-NODAGA-HPβCD: 2.65% ± 0.51%ID/g) was followed by a slight decrease until the 20th day ([^{68}Ga]Ga-DOTAGA-RAMEB: 2.35% ± 0.38%ID/g, [^{68}Ga]Ga-NODAGA-HPβCD: 2.11% ± 0.4%ID/g). In addition, the T41 tumor uptake of [^{68}Ga]Ga-DOTAGA-RAMEB slightly exceeded that of [^{68}Ga]Ga-NODAGA-HPβCD at all time points; however, the differences did not reach statistical significance.

For the MDA-MB-HER2+ tumors (Table S4 and Figure 5 Panel B), the HPβCD compound demonstrated significantly higher

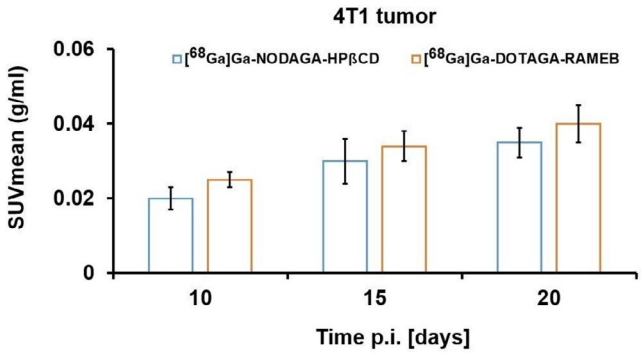

FIGURE 4 | Quantitative PET analysis of mice bearing triple negative 4T1 tumors. Results of quantitative SUV analysis 10, 15, and 20 days after tumor induction and 60 min post tail-vein injection of [^{68}Ga]Ga-NODAGA-HPβCD and [^{68}Ga]Ga-DOTAGA-RAMEB in CB17 SCID mice bearing 4T1 tumors. All values are expressed as mean ± SD. $n = 3$ mice/radiotracer/time point. SUV values for [^{68}Ga]Ga-NODAGA-HPβCD were 0.02 ± 0.003, 0.03 ± 0.006, and 0.035 ± 0.004 g/mL 10, 15, and 20 days post tumor cell transplantation, respectively. For [^{68}Ga]Ga-DOTAGA-RAMEB, corresponding SUV values were 0.025 ± 0.002, 0.034 ± 0.004, and 0.04 ± 0.005 g/mL. p.i., Post injection of 4T1 tumor cells; SUV, standardized uptake value.

accumulation ($p \leq 0.05$) compared to the RAMEB molecule at the first two investigation time points (35th day: 2.727% ± 0.48%ID/g and 5.779% ± 1.06%ID/g for [^{68}Ga]Ga-DOTAGA-RAMEB

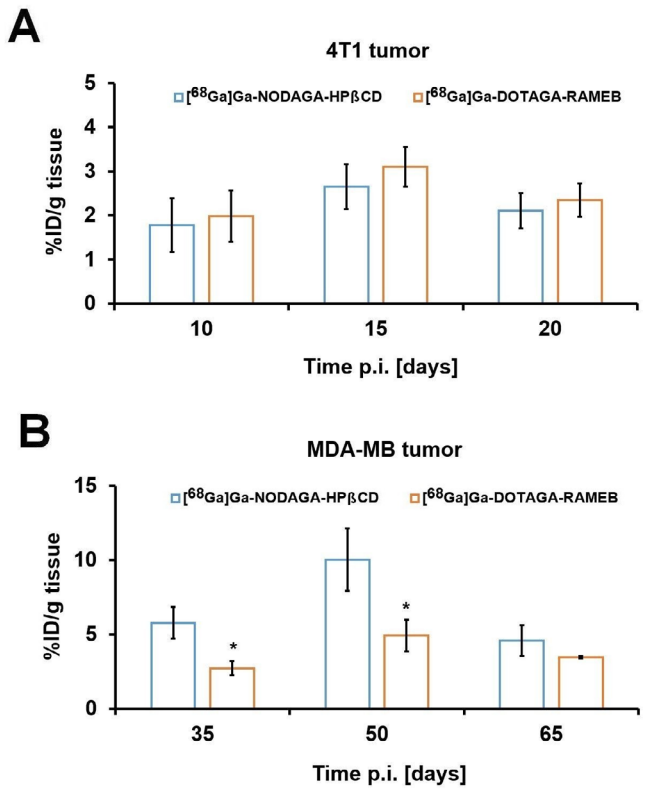

FIGURE 5 | Results of post-imaging biodistribution studies with triple negative 4T1 and MDA-MB-HER2+ breast tumors. Ex vivo biodistribution data of [^{68}Ga]Ga-NODAGA-HPβCD and [^{68}Ga]Ga-DOTAGA-RAMEB in 4T1 (Panel A) and MDA-MB-HER2+ (Panel B) tumors 60 min after tracer injection and 10, 15, 20 (4T1)/35, 50, 65 (MDA-MB-HER2+) days post tumor cell inoculation (p.i.). 3 animals/radiopharmaceuticals/time point. *$p \leq 0.05$. %ID/g values are expressed as mean ± SD. p.i., post injection of tumor cells.

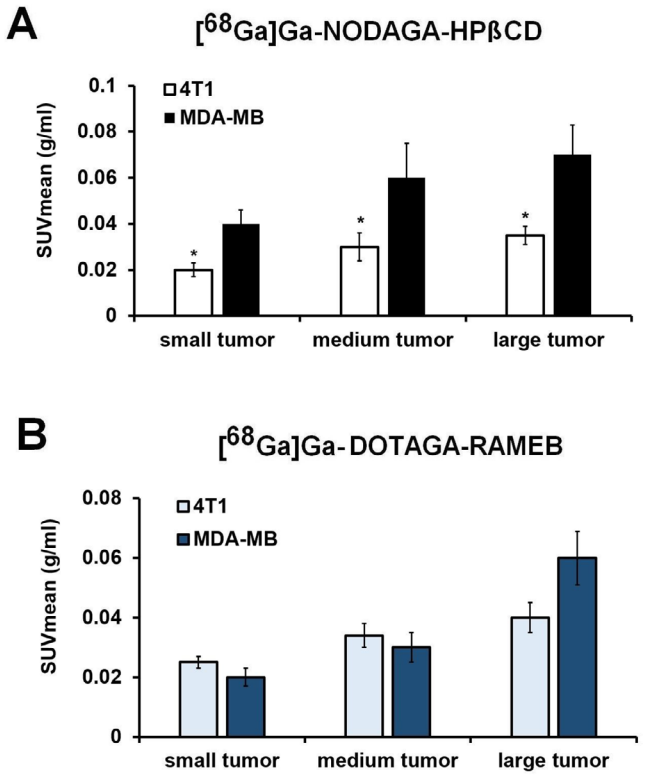

FIGURE 6 | Radiopharmaceutical accumulation in tumors depending on tumor size. Tumor size-dependent comparison of [^{68}Ga]Ga-NODAGA-HPβCD (Panel A) and [^{68}Ga]Ga-DOTAGA-RAMEB (Panel B) accumulation in MDA-MB-HER2+ and 4T1 tumors. SUV values (g/mL) are expressed as mean ± SD. SUV, standardized uptake value.

and [^{68}Ga]Ga-NODAGA-HPβCD; respectively; 50th day: 4.929% ± 1.06%ID/g and 10.039% ± 2.09%ID/g for [^{68}Ga]Ga-DOTAGA-RAMEB and [^{68}Ga]Ga-NODAGA-HPβCD; respectively). Sixty-five days after tumor establishment, the tumor concentration was still slightly more elevated for [^{68}Ga]Ga-NODAGA-HPβCD than for RAMEB; however, the difference was statistically not meaningful. The radiopharmaceutical uptake tendency of the MDA-MB-HER2+ tumors mirrored that of the 4T1 tumors, with increasing %ID/g data until the 2nd time point, followed by a decline until the end of the experiment (Figure 5, Panel B).

3.3 | Comparison of [^{68}Ga]Ga-NODAGA-HPβCD and [^{68}Ga]Ga-DOTAGA-RAMEB Accumulation in MDA-MB-HER2+ and 4T1 Tumors

Finally, the in vivo uptake of [^{68}Ga]Ga-NODAGA-HPβCD and [^{68}Ga]Ga-DOTAGA-RAMEB was also compared within each tumor size category (small, medium-sized, and large tumors) (Figure 6).

Based on SUV data analysis, the accumulation of [^{68}Ga]Ga-NODAGA-HPβCD was significantly higher in the small MDA-MB-HER2+ tumors compared to size-matched 4T1 tumors *($p \leq 0.05$)* (Figure 6, Panel A). Nevertheless, the tracer concentrations showed a gradual increase; this trend persisted for medium and large tumors, with MDA-MB-HER2+ tumors surpassing the radioactivity of the 4T1 tumors, and these differences were also statistically significant *($p \leq 0.05$)*.

As for the RAMEB derivative, the small and midsized 4T1 tumors accumulated the compound to a greater extent in comparison with the MDA-MB-HER2+ counterparts. Conversely, regarding the large tumors, its uptake was higher in the HER2+ lesions (Figure 6, Panel B). Of note, these activity differences did not reach statistical significance.

3.4 | Assessment of Tumor Growth Dynamics

Parallel with the in vivo studies, the intrinsic growth potential of the two different tumors was also assessed (Figure 7). The tumor growth curve of the 4T1 tumors showed rapid cell proliferation kinetics and exponentially increasing tumor sizes, with respective values being 75 ± 13 mm^3, 212 ± 24 mm^3 and 342 ± 30 mm^3 10, 15, and 20 days post tumor establishment. In contrast, the MDA-MB-HER2+ tumors grew more slowly and reached volumes of 30 ± 4 mm^3, 79 ± 11 mm^3, and 128 ± 22 mm^3 35, 50, and 65 days after tumor cell inoculation, respectively. Figure 7 presents the comparison of the growth dynamics of the two tumors with different biological behavior.

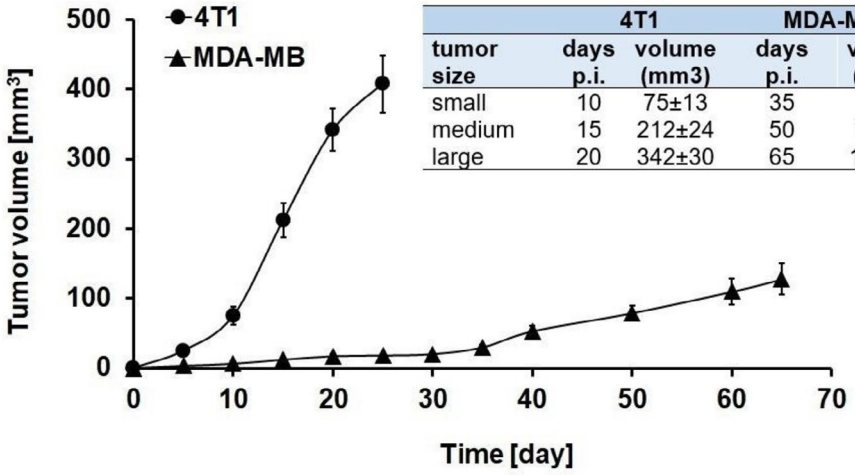

	4T1		MDA-MB	
tumor size	days p.i.	volume (mm3)	days p.i.	volume (mm3)
small	10	75±13	35	30±4
medium	15	212±24	50	79±11
large	20	342±30	65	128±22

FIGURE 7 | Proliferation kinetics of 4T1 and MDA-MB-HER2+ tumors. Comparison of the growth dynamics of 4T1 and MDA-MB-HER2+ tumors. The tumor growth curve indicates rapid growing potential for the aggressive 4T1 tumors and gradual development for the HER2+ tumors. The proliferation differences between the two tumor models are demonstrated in the inserted table on the right via examples of three growth phases (small, medium-size, and large tumors).

4 | Discussion

Given the crucial role of PGE2 and its receptors in guiding tumor-related angiogenesis, we hypothesized that biomolecules addressing these factors would widen the armamentarium of direct angiogenesis-targeting agents for breast cancer molecular imaging. Encouraging former findings on radiolabelled cyclodextrin derivatives to identify tumors with PGE2 overexpression [33, 34] prompted us to test and compare the feasibility of ^{68}Ga-labeled cyclodextrins for in vivo breast cancer detection.

Our results indicating notable radioactivity in both 4T1 and MBA-MD-HER2+ tumors designate [^{68}Ga]Ga-DOTAGA-RAMEB and [^{68}Ga]Ga-NODAGA-HPβCD as effective PET probes for breast cancer imaging. This is the first study to report on the applicability of cyclodextrin radioprobes in mamma imaging, complementing earlier preclinical works [33, 34, 35, 36] where radiolabelled versions of RAMEB and HPβCD molecules (^{68}Ga, ^{213}Bi or ^{52}Mn) were successfully used to detect different tumor types such as fibrosarcoma, B-cell lymphoma, malignant melanoma, pancreatic adenocarcinoma, or mesoblastic nephroma with PET technique [33–36].

Considering the inert complex-forming ability of cyclodextrins with PGE2 [31, 36], the detected tumor uptakes may reflect PGE2 positivity in these breast cancer models, consistent with previous findings in 4T1 cell lines [37]. Nevertheless, the exact PGE2 expression profile of the used tumors is not yet fully established; our data suggest that tumor radioactivities could correlate with peritumoral PGE2 concentrations and PGE2 receptorial expression. This aligns with the findings of Szabó et al. (2023), who reported a direct association between [^{68}Ga]Ga-DOTAGA-RAMEB/[^{68}Ga]Ga-NODAGA-HPβCD uptake and immunohistochemically determined PGE2 levels across several preclinical tumor models, including, among others, B16F10 melanoma, A20 lymphoma, or BxPC-3 pancreatic adenocarcinoma [36].

Although the tumor tracer uptakes could be in association with the presence of PGE2 and its receptors, it remains part of future work to investigate the background of the uptake differences between the two tracers in the 4T1 and in the MDA-MB-HER2+ tumors. In this respect, we suppose that differences between the target affinity of the RAMEB and HPβCD molecules and the possible non-specific activities could in part explain the reason behind it. Furthermore, pharmacokinetical variances between the two cyclodextrins and related different wash-out dynamics may also be accountable for the differences between the uptake patterns of the probes within one tumor.

Despite these intratumoral uptake differences, both tracers showed steadily increasing tumor accumulations over time. Even if detailed IHC analyses are necessary for complete verification, we hypothesize that enhanced angiogenesis coupled with elevated levels of pro-angiogenic factors (PGE2 and receptors) contribute to this trend, potentially indicating aggravated malignancy and higher metastatic potential. Finally, tracer uptakes between the two tumor types could not be directly compared because of the different acquisition time points (4T1: 10, 15, 20 days and MDA-MB-HER2+: 35, 50, 65 days post tumor cell injection).

In the second part of our study, we assessed tumor growth kinetics and tracer uptakes across tumors of varying sizes (small, medium, and large). Based on the results, we conclude that both ^{68}Ga-cyclodextrins could be used for breast cancer diagnostics regardless of the growing potential, as both the rapidly growing 4T1 and the slower MDA-MB tumors accumulated detectable radioactivity at all scanning times.

Despite being feasible to identify breast cancer, the diagnostic performance of [^{68}Ga]Ga-DOTAGA-RAMEB and [^{68}Ga]Ga-NODAGA-HPβCD varied with tumor type and size, which could have significant clinical implications. PET data revealed that the HPβCD compound seemed to perform better in the

imaging of HER2+ breast cancers irrespective of size. Unlike, in the case of the RAMEB derivative, tumor-homing was highly affected by tumor bulk—favoring small and mid-sized 4T1 lesions and large MDA-MB tumors. Despite variances in size-dependent tumor radioactivities, for large tumors, both tracers better visualized MDA-MB breast cancer than 4T1 tumors. We suggest that compared to the receptor-positive MDA-MB tumors, the more aggressive nature of the triple-negative tumors leads to earlier tumor dedifferentiation and related reduced angiogenesis, which eventually results in lower PGE2/receptor levels and cyclodextrin uptake. Additionally, the differences in scanning times, the presence of hypoxia, or chronic inflammation may also influence the individual tumor activities.

Finally, by targeting PGE2 and its receptors, radiolabelled cyclodextrins offer a novel, highly specific alternative to the gold-standard [^{18}F]FDG-PET. This molecular specificity not only overcomes key limitations of [^{18}F]FDG—such as lack of specificity or reduced sensitivity in certain breast cancer subtypes (e.g., lobular or low-grade tumors)—but, considering the prognostic relevance of PGE2/receptors in gynecological malignancies, may also yield important prognostic insights [38, 39]. In addition, cyclodextrin-based tracers may be particularly valuable in tumors with low or variable [^{18}F]FDG uptake or in clinical contexts where angiogenesis is a major driver of disease progression, thereby broadening the spectrum of molecular probes available for breast cancer imaging. Moreover, their compatibility with therapeutic radionuclides positions cyclodextrins as versatile theranostic agents capable of combining precise diagnosis with targeted treatment options.

5 | Conclusion

In summary, this is the first study so far to report on the diagnostic feasibility of radiolabelled cyclodextrin molecules in the in vivo detection of breast cancer. Based on our pioneering results, ^{68}Ga-labeled cyclodextrins may be part of diagnostic tools in future breast cancer imaging, especially in receptor-negative malignancies. Although further experiments are straightforward to confirm the association between cyclodextrin uptake and PGE2 expression, [^{68}Ga]Ga-DOTAGA-RAMEB and [^{68}Ga]Ga-NODAGA-HPβCD may be usefully applied in the design and development of novel carbohydrate-mediated vascular-targeting agents for mamma imaging.

Author Contributions

Z.K. and G.T. wrote the manuscript; T.S., G.T., and I.H. designed the research; J.P.S. and R.A.D. performed the research; T.S., Z.K., P.Á., and F.F. analyzed the data; A.F., I.J., and G.O. contributed new reagents/analytical tools.

Acknowledgments

The authors acknowledge the use of artificial intelligence tools to assist in language editing.

Conflicts of Interest

The authors declare no conflicts of interest.

References

1. S. Loibl, P. Poortmans, M. Morrow, C. Denkert, and G. Curigliano, "Breast Cancer," *Lancet* 397 (2021): 1750–1769, https://doi.org/10.1016/S0140-6736(20)32381-3.

2. W. Xu, T. Zhang, Z. Zhu, and Y. Yang, "The Association Between Immune Cells and Breast Cancer: Insights From Mendelian Randomization and Meta-Analysis," *International Journal of Surgery* 111 (2025): 230–241, https://doi.org/10.1097/JS9.0000000000001840.

3. R. L. Siegel, A. N. Giaquinto, and A. Jemal, "Cancer Statistics," *Cancer Journal for Clinicians* 74 (2024): 12–49, https://doi.org/10.3322/caac.21820.

4. O. Ginsburg, C. H. Yip, A. Brooks, et al., "Breast Cancer Early Detection: A Phased Approach to Implementation," *Cancer* 126 (2020): 2379–2393, https://doi.org/10.1002/cncr.32887.

5. J. M. Seely, "Progress and Remaining Gaps in the Early Detection and Treatment of Breast Cancer," *Current Oncology* 30 (2023): 3201–3205, https://doi.org/10.3390/curroncol30030242.

6. M. Bernsdorf, A. K. Berthelsen, V. T. Wielenga, et al., "Preoperative PET/CT in Early-Stage Breast Cancer," *Annals of Oncology* 23 (2012): 2277–2282, https://doi.org/10.1093/annonc/mds002.

7. W. J. Gradishar, B. O. Anderson, R. Blassanian, et al., "NCCN Clinical Practice Guidelines in Oncology (NCCN Guidelines) Breast Cancer," (2015), http://www.nccn.org/professionals/physician_gls/pdf/breast.pdf.

8. G. N. Nursal, T. Z. Nursal, H. O. Aytac, et al., "Is PET/CT Necessary in the Management of Early Breast Cancer?," *Clinical Nuclear Medicine* 41 (2016): 362–365, https://doi.org/10.1097/RLU.0000000000001165.

9. T. S. Aukema, E. J. Rutgers, W. V. Vogel, et al., "The Role of FDG PET/CT in Patients With Locoregional Breast Cancer Recurrence: A Comparison to Conventional Imaging Techniques," *European Journal of Surgical Oncology* 36 (2010): 387–392, https://doi.org/10.1016/j.ejso.2009.11.009.

10. S. Avril, R. F. Muzic, D. Plecha, B. J. Traughber, S. Vinayak, and N. Avril, "^{18}F-FDG PET/CT for Monitoring of Treatment Response in Breast Cancer," *Journal of Nuclear Medicine* 57, no. 1 (2016): 34S–39S, https://doi.org/10.2967/jnumed.115.157875.

11. D. de Jong, E. Desperito, K. A. Al Feghali, et al., "Advances in PET/CT Imaging for Breast Cancer," *Journal of Clinical Medicine* 12 (2023): 4537, https://doi.org/10.3390/jcm12134537.

12. N. M. Toàn, "Novel Molecular Classification of Breast Cancer With PET Imaging," *Medicina (Kaunas, Lithuania)* 60 (2024): 2099, https://doi.org/10.3390/medicina60122099.

13. C. M. de Mooij, R. A. W. Ploumen, P. J. Nelemans, F. M. Mottaghy, M. L. Smidt, and T. J. A. van Nijnatten, "The Influence of Receptor Expression and Clinical Subtypes on Baseline [18F]FDG Uptake in Breast Cancer: Systematic Review and Meta-Analysis," *EJNMMI Research* 13 (2023): 5, https://doi.org/10.1186/s13550-023-00953-y.

14. R. Kumar, A. Chauhan, H. Zhuang, P. Chandra, M. Schnall, and A. Alavi, "Clinicopathologic Factors Associated With False Negative FDG–PET in Primary Breast Cancer," *Breast Cancer Research and Treatment* 98 (2006): 267–274, https://doi.org/10.1007/s10549-006-9159-2.

15. H. O'Neill, V. Malik, C. Johnston, J. V. Reynolds, and J. O'sullivan, "Can the Efficacy of [18F]FDG-PET/CT in Clinical Oncology be Enhanced by Screening Biomolecular Profiles?," *Pharmaceuticals* 12 (2019): 16, https://doi.org/10.3390/ph12010016.

16. B. McKnight, S. Kim, J. L. Boerner, and N. T. Viola, "Cetuximab PET Delineated Changes in Cellular Distribution of EGFR Upon Dasatinib Treatment in Triple Negative Breast Cancer," *Breast Cancer Research* 22 (2020): 37, https://doi.org/10.1186/s13058-020-01270-1.

17. C. Liu, C. Gong, S. Liu, et al., "18F-FES PET/CT Influences the Staging and Management of Patients With Newly Diagnosed Estrogen

Receptor-Positive Breast Cancer: A Retrospective Comparative Study With 18F-FDG PET/CT," *Oncologist* 24 (2019): e1277–e1285, https://doi.org/10.1634/theoncologist.2019-0096.

18. H. Hong, Y. Zhang, T. R. Nayak, et al., "Immuno-PET of Tissue Factor in Pancreatic Cancer," *Journal of Nuclear Medicine* 53 (2012): 1748–1754, https://doi.org/10.2967/jnumed.112.105460.

19. S. M. Okarvi and I. Al Jammaz, "Preparation and Evaluation of the Tumor-Specific Antigen-Derived Synthetic Mucin 1 Peptide: A Potential Candidate for the Targeting of Breast Carcinoma," *Nuclear Medicine and Biology* 43 (2016): 403–409, https://doi.org/10.1016/j.nucmedbio.2016.03.006.

20. C. A. Ferreira, L. Kang, C. Li, et al., "ImmunoPET of the Differential Expression of CD146 in Breast Cancer," *American Journal of Cancer Research* 11 (2021): 1586–1599.

21. P. Backhaus, M. C. Burg, W. Roll, et al., "Simultaneous FAPI PET/MRI Targeting the Fibroblast-Activation Protein for Breast Cancer," *Radiology* 302 (2022): 39–47, https://doi.org/10.1148/radiol.2021204677.

22. S. Kakarla, X. T. Song, and S. Gottschalk, "Cancer-Associated Fibroblasts as Targets for Immunotherapy," *Immunotherapy* 4 (2012): 1129–1138, https://doi.org/10.2217/imt.12.112.

23. J. Cheng, L. Lei, J. Xu, et al., "18F-Fluoromisonidazole PET/CT: A Potential Tool for Predicting Primary Endocrine Therapy Resistance in Breast Cancer," *Journal of Nuclear Medicine* 54 (2013): 333–340, https://doi.org/10.2967/jnumed.112.111963.

24. S. Lee, V. Muralidharan, N. Tebbutt, et al., "Prevalence of Hypoxia and Correlation With Glycolytic Metabolism and Angiogenic Biomarkers in Metastatic Colorectal Carcinoma," *European Journal of Nuclear Medicine and Molecular Imaging* 48 (2021): 1585–1592, https://doi.org/10.1007/s00259-020-05074-5.

25. S. Lopes, S. Ferreira, and M. Caetano, "PET/CT in the Evaluation of Hypoxia for Radiotherapy Planning in Head and Neck Tumors: Systematic Literature Review," *Journal of Nuclear Medicine Technology* 49 (2021): 107–113, https://doi.org/10.2967/jnmt.120.249540.

26. R. Chakravarty, S. Chakraborty, and A. Dash, "Molecular Imaging of Breast Cancer: Role of RGD Peptides," *Mini Reviews in Medicinal Chemistry* 15 (2015): 1073–1094, https://doi.org/10.2174/1389557515666150909144606.

27. S. B. Gaykema, A. H. Brouwers, M. N. de Lub- Hooge, et al., "89Zr-Bevacizumab PET Imaging in Primary Breast Cancer," *Journal of Nuclear Medicine* 54 (2013): 1014–1018, https://doi.org/10.2967/jnumed.112.117218.

28. A. Florea, F. M. Mottaghy, and M. Bauwens, "Molecular Imaging of Angiogenesis in Oncology: Current Preclinical and Clinical Status," *International Journal of Molecular Sciences* 22 (2021): 5544, https://doi.org/10.3390/ijms22115544.

29. E. Half, X. M. Tang, K. Gwyn, A. Sahin, K. Wathen, and F. A. Sinicrope, "Cyclooxygenase-2 Expression in Human Breast Cancers and Adjacent Ductal Carcinoma In Situ," *Cancer Research* 62 (2002): 1676–1681.

30. F. Hirayama, M. Kurihara, and K. Uekama, "Improving the Aqueous Stability of Prostaglandin E2 and Prostaglandin A2 by Inclusion Complexation With Methylated-Beta-Cyclodextrins," *Chemical and Pharmaceutical Bulletin* 32 (1984): 4237–4240, https://doi.org/10.1248/cpb.32.4237.

31. R. S. Sauer, H. L. Rittner, N. Roewer, et al., "A Novel Approach for the Control of Inflammatory Pain: Prostaglandin E2 Complexation by Randomly Methylated β-Cyclodextrins," *Anesthesia and Analgesia* 124 (2017): 675–685, https://doi.org/10.1213/ANE.0000000000001674.

32. I. Hajdu, J. Angyal, D. Szikra, et al., "Radiochemical Synthesis and Preclinical Evaluation of ^{68}Ga-Labeled NODAGA-Hydroxypropyl-Beta-Cyclodextrin (^{68}Ga-NODAGA-HPBCD)," *European Journal of Pharmaceutical Sciences* 128 (2019): 202–208, https://doi.org/10.1016/j.ejps.2018.12.001.

33. G. Trencsényi, A. Kis, J. P. Szabó, et al., "In Vivo Preclinical Evaluation of the New ^{68}Ga-Labeled Beta-Cyclodextrin in Prostaglandin E2 (PGE2) Positive Tumor Model Using Positron Emission Tomography," *International Journal of Pharmaceutics* 576 (2020): 118954, https://doi.org/10.1016/j.ijpharm.2019.118954.

34. K. Csige, J. P. Szabó, I. Kálmán-Szabó, et al., "In Vivo Investigation of Gallium-68 and Bismuth-205/206 Labeled Beta Cyclodextrin for Targeted Alpha Therapy of Prostaglandin E2 Receptor-Expressing Tumors in Mice," *International Journal of Pharmaceutics* 625 (2022): 122132, https://doi.org/10.1016/j.ijpharm.2022.122132.

35. Z. Képes, J. P. Szabó, I. Kálmán-Szabó, et al., "^{52}Mn-Labelled Beta-Cyclodextrin for Melanoma Imaging: A Proof-Of-Concept Preclinical Study," *In Vivo* 38 (2024): 2591–2600, https://doi.org/10.21873/invivo.13735.

36. J. P. Szabó, K. Csige, I. Kálmán-Szabó, et al., "In Vivo Assessment of Tumor Targeting Potential of ^{68}Ga-Labelled Randomly Methylated Beta-Cyclodextrin (RAMEB) and 2-Hydroxypropyl-β-Cyclodextrin (HPβCD) Using Positron Emission Tomography," *International Journal of Pharmaceutics* 630 (2023): 122462, https://doi.org/10.1016/j.ijpharm.2022.122462.

37. M. Mitsuhashi, J. Liu, S. Cao, X. Shi, and X. Ma, "Regulation of Interleukin-12 Gene Expression and Its Anti-Tumor Activities by Prostaglandin E2 Derived From Mammary Carcinomas," *Journal of Leukocyte Biology* 76 (2004): 322–332, https://doi.org/10.1189/jlb.1203641.

38. S. Dietlmeier, Y. Ye, C. Kuhn, et al., "The Prostaglandin Receptor EP2 Determines Prognosis in EP3-Negative and Galectin-3-High Cervical Cancer Cases," *Scientific Reports* 10 (2020): 1154, https://doi.org/10.1038/s41598-020-58095-3.

39. A. Semmlinger, V. von Schoenfeldt, V. Wolf, et al., "EP3 (Prostaglandin E2 Receptor 3) Expression Is a Prognostic Factor for Progression-Free and Overall Survival in Sporadic Breast Cancer," *BMC Cancer* 18 (2018): 431, https://doi.org/10.1186/s12885-018-4286-9.

Supporting Information

Additional supporting information can be found online in the Supporting Information section. **Data S1:** cts70379-sup-0001-Supinfo.docx.